Available online at www.sciencedirect.com
ScienceDirect
Applied Mathematical Modelling 32 (2008) 1445–1462
APPLIED MATHEMATICAL MODELLING
www.elsevier.com/locate/apm

Mathematical simulation of combined trajectory paths of a seven link biped robot

Peiman Naseradin Mousavi [a,*], C. Nataraj [b], Ahmad Bagheri [a], Mahdi Alizadeh Entezari [c]

[a] Department of Mechanical Engineering, Guilan University, Rasht, Iran
[b] Department of Mechanical Engineering, Villanova University, Villanova, USA
[c] Department of Mechanical Engineering, Amir Kabir University, Tehran, Iran

Received 1 July 2006; received in revised form 1 October 2007; accepted 21 November 2007
Available online 4 December 2007

Abstract

The following article focuses on biped robot simulation and control over combined trajectory paths with the aid of mathematical modeling methods focusing on the effects of hip height over torso's modified motion. The mathematical simulation has been exploited to interpolate the combined trajectory of the robot path with the given breakpoints using inverse kinematic and dynamic methods to determine ZMP and stability treatments. After the robot's combined path determination, a third-order spline is utilized because of its high precision and ability to calculate the kinematic, dynamic and control parameters. With the aid of this software, common parameters such as joint angles and inertial forces for the given specifications and nominal conditions are calculated and simulated.

Keywords: Seven link biped robot; Combined trajectory planning; Simulation; Third-order spline; Moving and fixed ZMP

1. Introduction

Numerous collaborations have been focused on single trajectory paths of the biped robot [1] while combined trajectory paths have not received much attention. In this paper, we have hence focused on generation of combined trajectory paths with the aid of mathematical interpolation. Zarrugh and Radcliffe [2] have considered a biped robot with respect to a walking pattern by recording human kinematic data while McGeer [3] have focused on passive walking of a biped robot generated by gravitational and inertial components. Silva and Machado [4] have focused on actuator power and energy by the adaptation of walking parameters. The stability of the robot is connected to the biped robot's tendency to tip over. Zheng and Shen [5] have considered a method of gait synthesis with respect to static stability while Chevallereau [6] have focused on

* Corresponding author.
E-mail addresses: payman.mousavi@gmail.com (P.N. Mousavi), nataraj@villanova.edu (C. Nataraj), Bagheri@guilan.ac.ir (A. Bagheri), mehdi.entezari@gmail.com (M.A. Entezari).

0307-904X/$ - see front matter © 2007 Elsevier Inc. All rights reserved.
doi:10.1016/j.apm.2007.11.026

dynamic stability with the aid of a low energy reference trajectory definition. Takanishi et al. [7], Shih et al. [8], Hirai et al. [9], and Dasgupta and Nakamura [10] have considered the robot dynamic stability with respect to the walking process based on the zero moment point (ZMP) method. With respect to the various conditions of combined trajectory paths, Shih [11,12], Huang et al. [13] utilized methods to generate the trajectory paths of the robot where they carried out simulation of the combined trajectory paths. The current article focuses on the inverse kinematic and dynamic methods for providing the robot combined trajectory paths in order to obtain a smooth motion of the robot. This procedure avoids the link's velocity discontinuities of the robot in order to mitigate the occurrence of impact effects and also helps to obtain a suitable control process. The main contribution of this work consists of a new method for simulation of a seven link biped robot over combined trajectory paths in order to study the effects of hip height over the torso's modified motion. The process has been performed based on the system given breakpoints and either third-order spline or Vandermonde matrix interpolation method. The employed methods generate the desired combined trajectory paths to avoid oscillation of the paths because of the high order of the polynomials. The simulations have been carried out for combined trajectory paths. Similar to human gait, the robot's feet make negative, zero and positive angles with the ground.

2. Kinematic modeling

The mathematical interpolation is one of the simplest methods utilized for obtaining the suitable curves with respect to the given break points that the robot must undergo. The process of inverse kinematics with the aid of the defined combined trajectory paths (they have been indicated by the operator) and also solving the nonlinear equations for the robot movement will result in the needed parameters. Parameters such as joint angles will be calculated for use in dynamics and the subsequent controlling equations before the actual calculation of the actuator torques. The actuator torques will be used in the indicated combined trajectory paths. In the current article, the simplest mathematical interpolations which are "Vandermonde matrix" and "third-order spline" [1,13] have been used. The mathematical equations of a biped robot are nonlinear systems of equations which contain complex mathematical relations. In Figs. 1 and 2, the robot saggital schematic has been presented to indicate the required nodes and the utility of the mentioned curves. With utilization of the specified criteria, the generated paths will be exploited in the designed software to obtain the kinematic parameters.

In general and with respect to Fig. 1, all the needed and important robot parameters are listed as follows:

(a) *Hip parameters*: The hip parameters include the vertical and horizontal displacements of the joint (z_h, x_h) and the variables which are displayed by Figs. 1 and 2, respectively. The distance between the hip and the fixed coordinate system (which is on the support leg) will be denoted for the instants of the beginning and the end points of the double support phase by x_{ed}, x_{sd}, respectively [13].

(b) *Foot parameters*: During the walking cycle, the horizontal and vertical displacements of ankle joint are displayed by x_a, z_a, respectively. The other parameters are as follows:

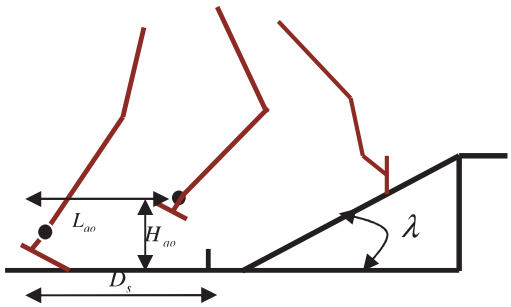

Fig. 1. The robot variables.

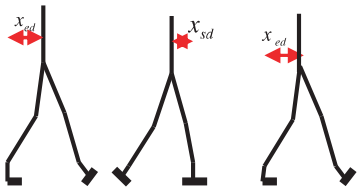

Fig. 2. The hip variables: x_{ed}, x_{sd}.

T_c	total traveling time including single and double support phases
T_d	double support phase time which is regarded as ≈20% of T_c
T_m	the time at which the ankle joint has reached the maximum height during the walking cycle
k	step number
H_{ao}	ankle joint maximum height
L_{ao}	the horizontal distance traveled between the ankle joint and the start point when the ankle joint has reached its maximum height
D_s	step length
q_b, q_f	foot lift angle and contact angle with the level ground
q_{gs}, q_{gf}	the ground initial terrain angles
h_{st}	stair level height
H_{st}	foot maximum height from stair level.

2.1. Trajectory of the robot

2.1.1. Foot trajectory interpolation

Five phases are required for calculation of the foot's combined trajectory path as shown in Fig. 3; they are derived in Appendix A. In the current process of the polynomial determination, boundary conditions of the movement play an important role for calculation of the combined trajectory paths. The required boundary conditions are derived with respect to the system requirements. Similar to the human walking process, foot angular velocity ($\dot{\theta}_a$) at the specified moments including the instants of the beginning and the end of foot traveling is equal to zero:

$$\dot{\theta}_a[t = kT_c, t = kT_c + T_d] = 0. \tag{5}$$

With respect to relations (1)–(4), a third-order spline can be utilized to provide the foot trajectory for the combined trajectory paths. Similar processes are exploited to calculate the trajectory paths for the displacements of horizontal and vertical foot traveling as shown below.

The displacement of the horizontal and vertical coordinates of the foot for the calculated breakpoints can be found in Appendices B and C, respectively.

In all the obtained relations, l_{ab}, l_{af} and l_{an} indicate the foot configuration as displayed in Fig. 4. H_s, h_s and St_{con} indicate the stair height, foot's maximum height measured from the stair level and the step number of the robot over the stair. The trajectory path of the hip follows the above utilized procedure with respect to walking of the robot phases [1]. The applicable constraints of the ankle and hip joints have been discussed in [1].

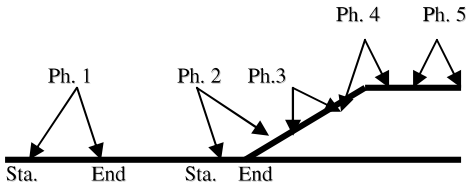

Fig. 3. The swing foot phases during gait.

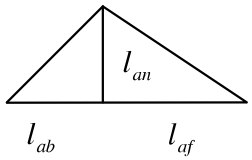

Fig. 4. The foot configuration.

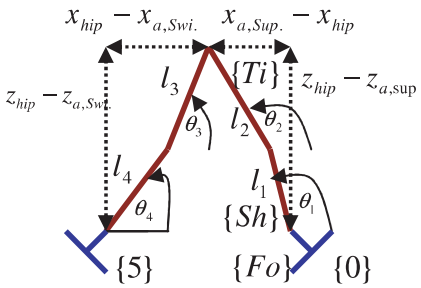

Fig. 5. The link's angles and configuration.

Now, the kinematic parameters will be obtained with respect to the above mentioned combined trajectory paths combined with the domain of the nonlinear equations (see Fig. 5). The nonlinear equations can be obtained as follows:

For support legs:

$$\begin{aligned} &l_1\cos(\pi-\theta_1)+l_2\cos(\pi-\theta_2)=a\\ &l_1\sin(\pi-\theta_1)+l_2\sin(\pi-\theta_2)=b \end{aligned} \tag{23}$$

For swing legs:

$$\begin{aligned} &l_3\cos(\theta_3)+l_4\cos(\theta_4)=c\\ &l_3\sin(\theta_3)+l_4\sin(\theta_4)=d. \end{aligned} \tag{24}$$

where

$$\begin{aligned} a &= x_{\mathrm{a,sup}}-x_{\mathrm{hip}}\\ b &= z_{\mathrm{hip}}-z_{\mathrm{a,sup}}\\ c &= x_{\mathrm{hip}}-x_{\mathrm{a,swing}}\\ d &= z_{\mathrm{hip}}-z_{\mathrm{a,swing}}. \end{aligned}$$

With the aid of the written programs and designed software, the above nonlinear equations based on the gait parameters are solved and also the link's angles are obtained. The kinematic parameters of the robot for single phase of the walking can be found in [1,14].

3. Dynamic investigations

With the biped's motion an important stability criteria (in similarities to the human gait) is defined using the zero moment point (ZMP). The ZMP is a point on the ground about which the sum of all the moments around is equal to zero. The ZMP formula is written as follows [13]:

$$x_{\mathrm{zmp}}=\frac{\sum_{i=1}^{n}m_i(g\ \cos\lambda+\ddot{z}_i)x_i-\sum_{i=1}^{n}m_i(g\ \sin\lambda+\ddot{x}_i)z_i-\sum_{i=1}^{n}{}^{i}I_i\ddot{\theta}_i}{\sum_{i=1}^{n}m_i(g\ \cos\ \lambda+\ddot{,}z_i)},$$

where $\ddot{x}_i, \ddot{z}_i$ are the vertical and horizontal acceleration of the mass center of link (i) with respect to the fixed coordinate system (which is on the support foot). $\ddot{\theta}_i$ is the angular acceleration of link (i) obtained from the interpolation process and λ denotes the slope of the surface. Principally, two types of ZMP are defined: (a) moving ZMP and (b) fixed ZMP.

The moving ZMP of the robot is similar to that for the human gait [1]. In the fixed type, the ZMP position is restricted through the support feet or the user's selected areas. Consequently, the significant torso's modified motion is required for stable walking of the robot. For the process here, the software has been designed to find the target angle of the torso for providing the fixed ZMP position automatically. In the designed software, q_{torso} shows the deflection angle of the torso determined by the user or calculated by the auto detector module of the software. Note that in the auto detector, the torso's motion needed for obtaining the mentioned fixed ZMP will be extracted with respect to the desired ranges. The desired ranges include the defined support feet area by the users or is determined automatically by the designed software. Note that the most affecting parameters for obtaining the robot's stable walking are the hip's height and position. By varying the parameters with an iterative method for x_{ed}, x_{sd} [13] and choosing the optimum hip height, the robot control process with respect to the torso's modified angles and the mentioned parameters can be performed. To obtain the joint's actuator torques, Lagrange equations [15] have been used at the single support phase as follows:

$$\tau_i = H(q)\ddot{q} + C(q,\dot{q})\dot{q} + G(q_i),$$

where $i = 0, 2, \ldots, 6$ and H, C, G are mass inertia, coriolis and gravitational matrices of the system which can be written as follows:

$$H(q) = \begin{bmatrix} h_{11} & h_{12} & h_{13} & h_{14} & h_{15} & h_{16} & h_{17} \\ h_{21} & h_{22} & h_{23} & h_{24} & h_{25} & h_{26} & h_{27} \\ h_{31} & h_{32} & h_{33} & h_{34} & h_{35} & h_{36} & h_{37} \\ h_{41} & h_{42} & h_{43} & h_{44} & h_{45} & h_{46} & h_{47} \\ h_{51} & h_{52} & h_{53} & h_{54} & h_{55} & h_{56} & h_{57} \\ h_{61} & h_{62} & h_{63} & h_{64} & h_{65} & h_{66} & h_{67} \end{bmatrix} \quad C(q,\dot{q}) = \begin{bmatrix} c_{11} & c_{12} & c_{13} & c_{14} & c_{15} & c_{16} & c_{17} \\ c_{21} & c_{22} & c_{23} & c_{24} & c_{25} & c_{26} & c_{27} \\ c_{31} & c_{32} & c_{33} & c_{34} & c_{35} & c_{36} & c_{37} \\ c_{41} & c_{42} & c_{43} & c_{44} & c_{45} & c_{46} & c_{47} \\ c_{51} & c_{52} & c_{53} & c_{54} & c_{55} & c_{56} & c_{57} \\ c_{61} & c_{62} & c_{63} & c_{64} & c_{65} & c_{66} & c_{67} \end{bmatrix}$$

$$G(q) = \begin{bmatrix} G_1 \\ G_2 \\ G_3 \\ G_4 \\ G_5 \\ G_{\text{tor}} \end{bmatrix}.$$

The most important point of the double support phase signifies the occurrence of the impact between the swing leg and the ground. Due to presence of the reaction force of the ground, Newton's equations must

Table 1
The simulated robot specifications

l_{Sh}	l_{Ti}	l_{To}	l_{an}	l_{ab}	l_{af}
0.3 m	0.3 m	0.3 m	0.1 m	0.1 m	0.13 m
m_{Sh}	m_{Th}	m_{To}	m_{Fo}	D_{s}	T_{c}
5.7 kg	10 kg	43 kg	3.3 kg	0.5 m	0.9 s
T_{d}	T_{m}	H_{ao}	L_{ao}	x_{ed}	x_{sd}
0.18 s	0.4 s	0.16 m	0.4 m	0.23 m	0.23 m
g_{gs}	g_{gf}	H_{min}	H_{max}	h_{s}	H_{s}
0	0	0.60 m	0.62 m	0.1 m	0.15 m
I_{shank}		I_{tight}		I_{torso}	I_{foot}
0.02 kg m^2		0.08 kg m^2		1.4 kg m^2	0.01 kg m^2
k_{Ch}		k_{Ch1}		k_{Ch2}	
2		5		7	

be employed for determination of the reaction force applied through the double support phase [13,16,17]. The method of [13] for simulation of the ground reaction force has been used for the inverse dynamics. Now, we have chosen an impeccable method involved slight deviations for dynamical analysis of the robot included the

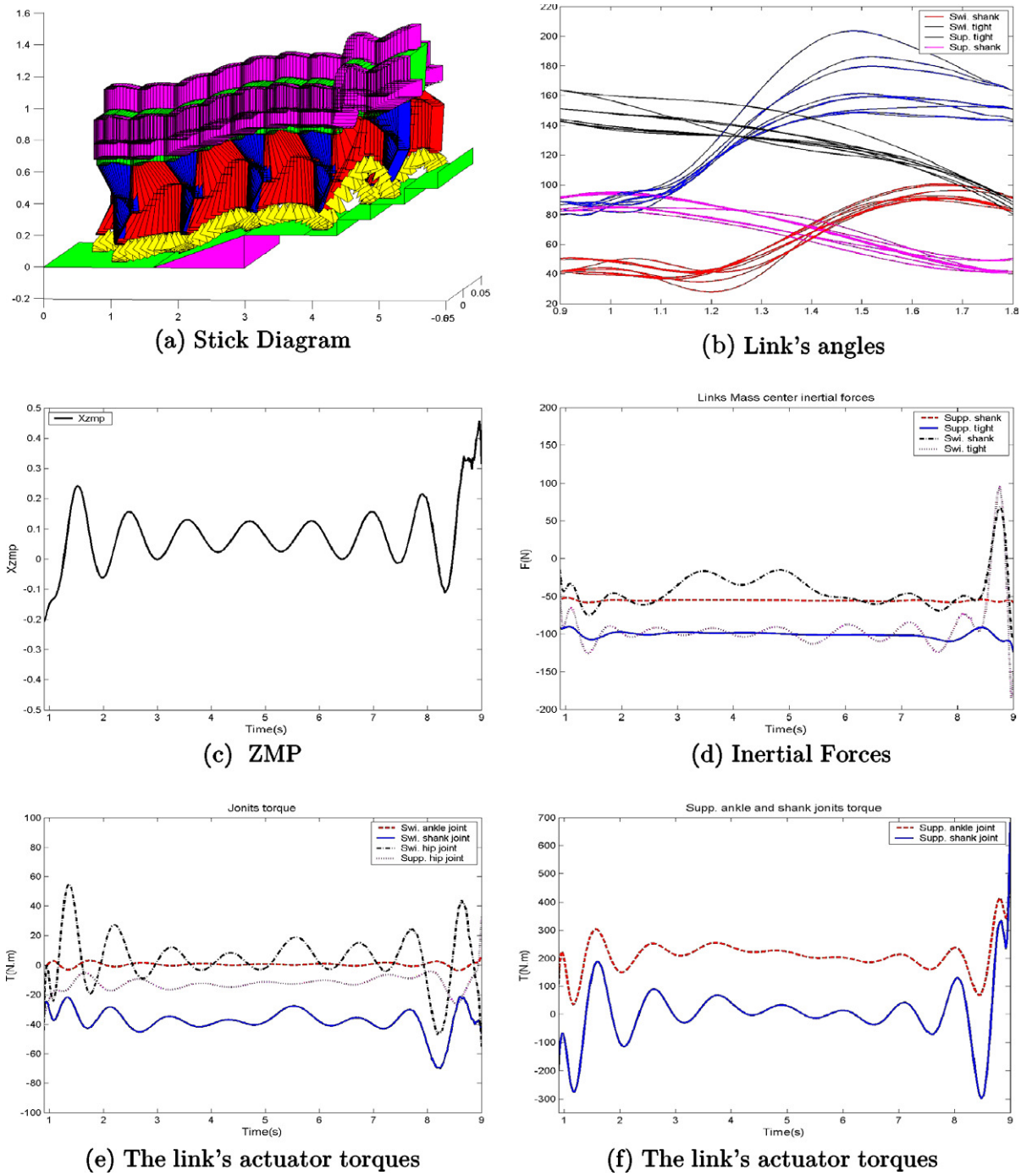

Fig. 6. (a) The robot's stick diagram on $\lambda = 8°$, moving ZMP, $H_{min} = 0.60$ m, $H_{max} = 0.62$ m; (b) the Link's angles during combined trajectory paths; (c) the moving ZMP diagram in nominal gait which satisfies stability criteria; (d) Inertial forces: (—) supp. tight, (- - -) supp. shank, (· · ·) swing tight, (·-·-·-) swing shank; (e) joint's torques: (—) swing shank joint, (- - -) swing ankle joint, (· · ·) supp. hip joint, (·-·-·-) swing hip joint; (f) joint's torques: (–) supp. ankle joint, (- - -) supp. shank joint.

Lagrangian and Newtonian relations. The components of the matrices are complex and the detailed mathematical relations can be found in [14].

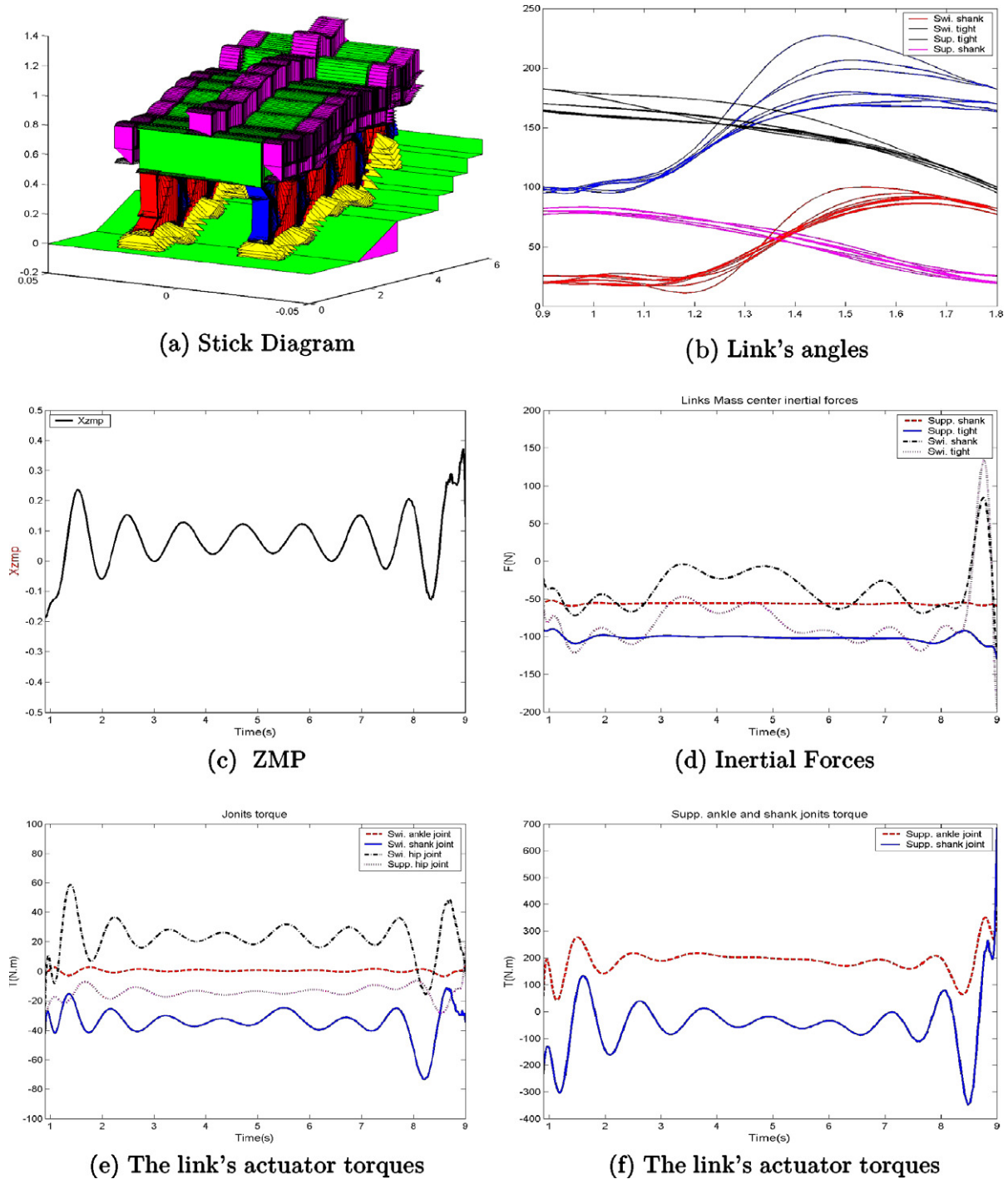

Fig. 7. (a) The robot's stick diagram on $\lambda = 8°$, moving ZMP, $H_{min} = 0.50$ m, $H_{max} = 0.52$ m. (b) The Link's angles during combined trajectory paths. (c) The moving ZMP diagram in nominal gait which satisfies stability criteria. (d) Inertial forces: (—) supp. tight, (- - -) supp. shank, (· · ·) swing tight, (-·-·-) swing shank. (e) Joint's torques (—) swing shank joint, (- - -) swing ankle joint, (· · ·) supp. hip joint, (-·-·-) swing hip joint. (f) Joint's torques: (—) supp. ankle joint, (- - -) supp. shank joint.

The following conditions must be applied during the simulation process:

- If $k \leqslant k_{\mathrm{Ch1}}$ and $k = k_{\mathrm{Ch2}} + 1$:

$$\lambda = 0$$

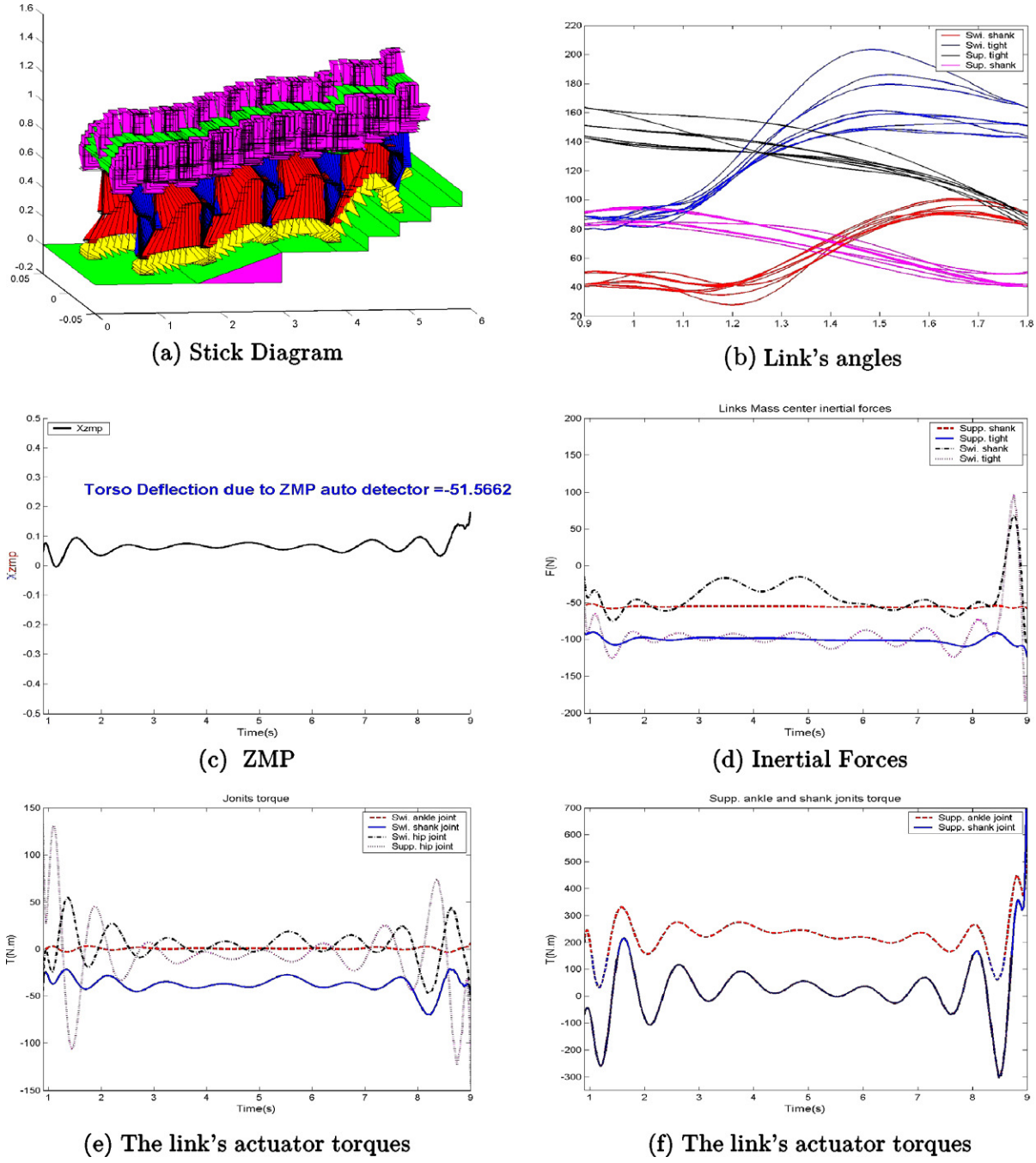

Fig. 8. (a) The robot's stick diagram on $\lambda = 8°$, fixed ZMP, $H_{\min} = 0.60$ m, $H_{\max} = 0.62$ m. (b) The Link's angles during combined trajectory paths. (c) The fixed ZMP diagram in nominal gait which satisfies stability criteria. (d) Inertial forces: (—) supp. tight, (- - -) supp. shank, (· · ·) swing tight, (-·-·-) swing shank. (e) Joint's torques (—) swing shank joint, (- - -) swing ankle joint, (· · ·) supp. hip joint, (-·-·-) swing hip joint. (f) Joint's torques: (—) supp. ankle joint, (- - -) supp. shank joint.

- If $k > k_{Ch1}$ and $k < k_{Ch2} + 1$:

  λ = The user defined value

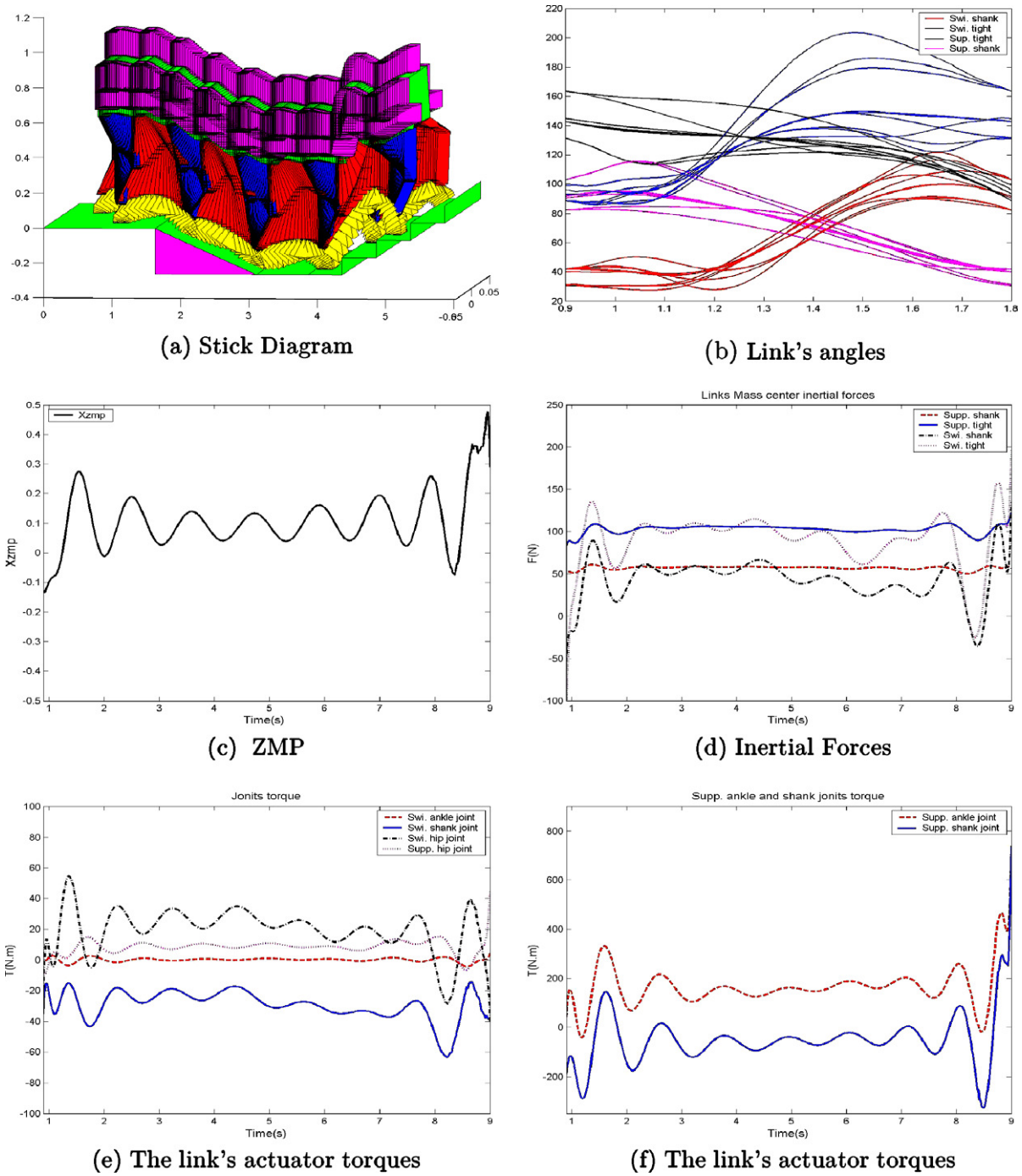

Fig. 9. (a) The robot's stick diagram on $\lambda = -10°$, moving ZMP, $H_{min} = 0.60$ m, $H_{max} = 0.62$ m. (b) The Link's angles during combined trajectory paths. (c) The moving ZMP diagram in nominal gait which satisfies stability criteria. (d) Inertial forces: (—) supp. tight, (- - -) supp. shank, (· · ·) swing tight, (·-·-·-) swing shank. (e) Joint's torques: (—) swing shank joint, (- - -) swing ankle joint, (· · ·) supp. hip joint, (·-·-·-) swing hip joint. (f) Joint's torques: (—) supp. ankle joint, (- - -) supp. shank joint.

where

Dec_{st} the number of robot's steps over the slope
k_{Ch} the number of steps that the robot changes during the walking process from the ground to slope

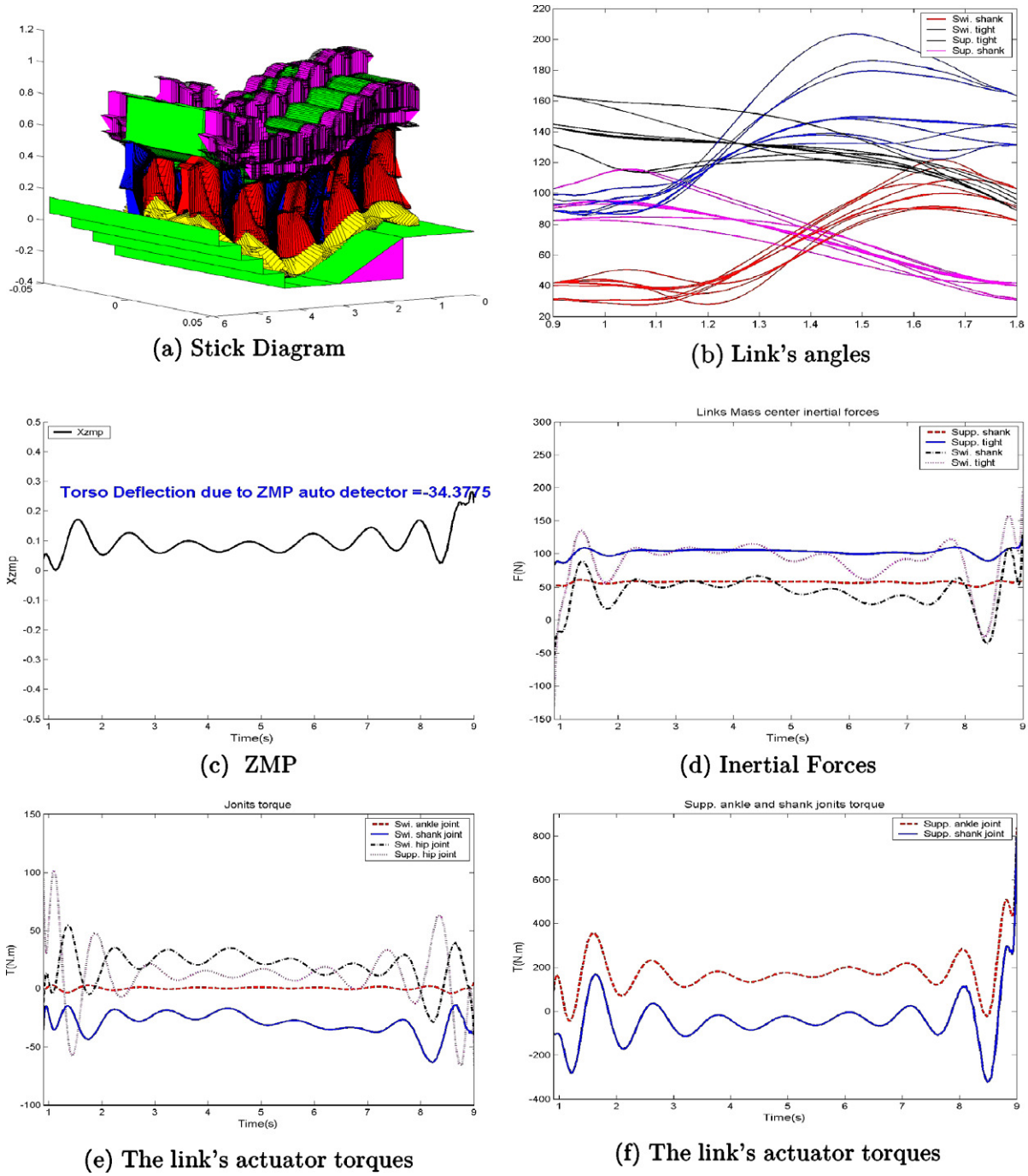

Fig. 10. (a) The robot's stick diagram on $\lambda = -10°$, fixed ZMP, $H_{min} = 0.60$ m, $H_{max} = 0.62$ m. (b) The Link's angles during combined trajectory paths. (c) The fixed ZMP diagram in nominal gait which satisfies stability criteria. (d) Inertial forces: (—) supp. tight, (- - -) supp. shank, (· · ·) swing tight, (·-·-·-) swing shank. (e) Joint's torques: (—) swing shank joint, (- - -) swing ankle joint, (· · ·) supp. hip joint, (·-·-·-) swing hip joint. (f) Joint's torques: (—) supp. ankle joint, (- - -) supp. shank joint.

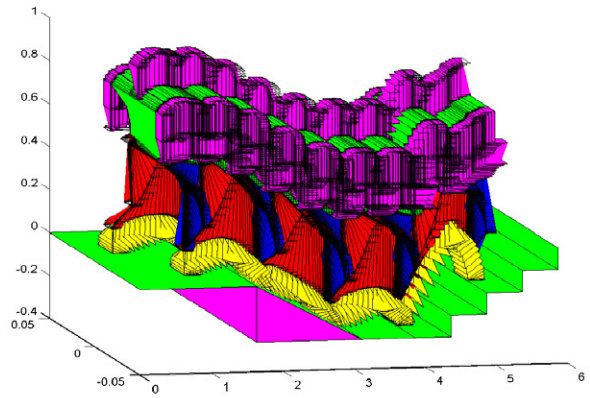

(a) Stick Diagram

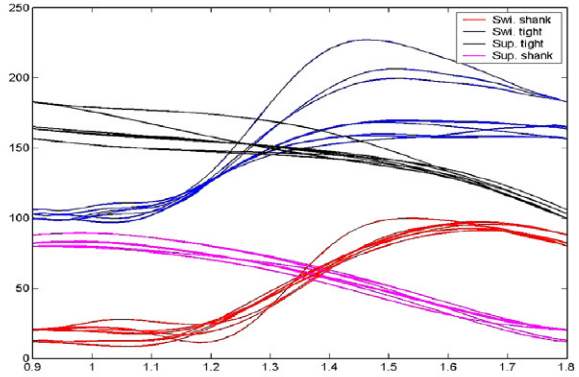

(b) Link's angles

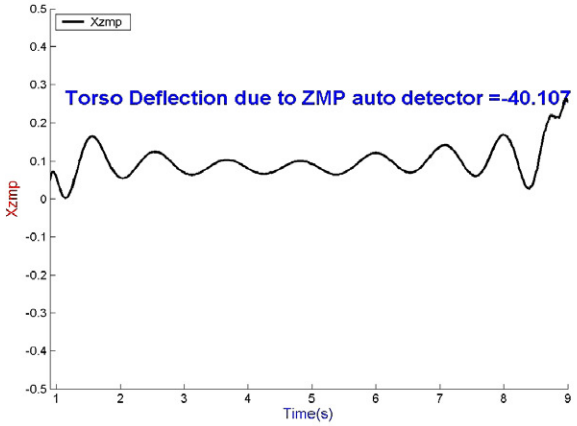

(c) ZMP

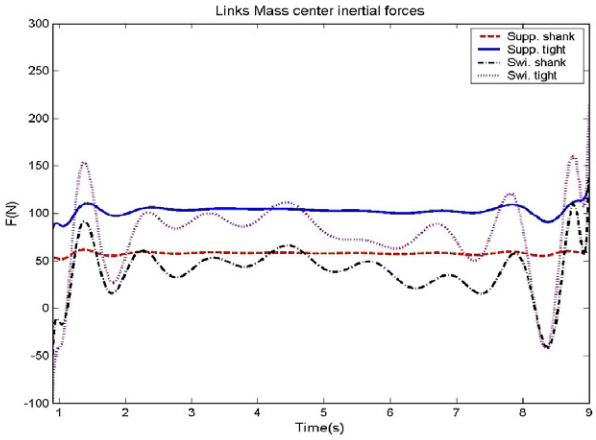

(d) Inertial Forces

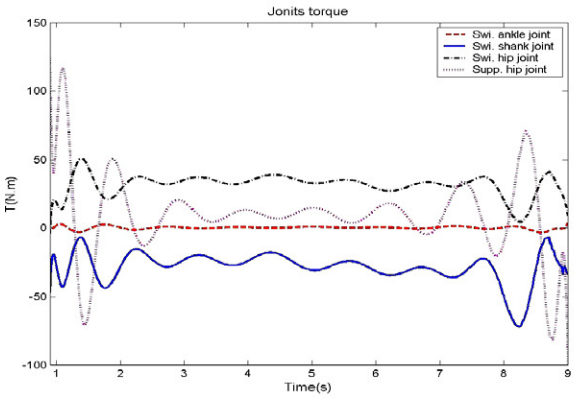

(e) The link's actuator torques

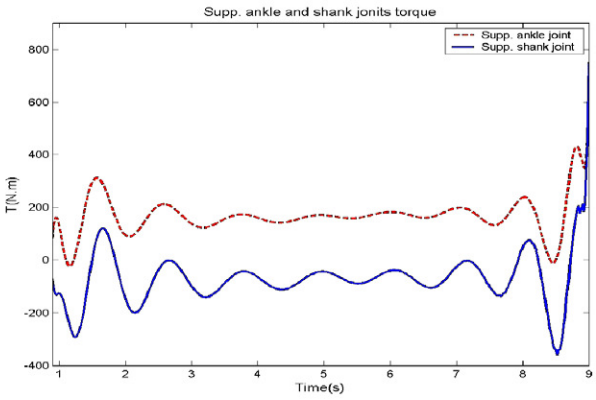

(f) The link's actuator torques

Fig. 11. (a) The robot's stick diagram on $\lambda = -10°$, fixed ZMP, $H_{\min} = 0.50$ m, $H_{\max} = 0.52$ m. (b) The Link's angles during combined trajectory paths. (c) The fixed ZMP diagram in nominal gait which satisfies stability criteria. (d) Inertial forces: (—) supp. tight, (- - -) supp. shank, (· · ·) swing tight, (·-·-·-) swing shank. (e) Joint's torques: (—) swing shank joint, (- - -) swing ankle joint, (· · ·) supp. hip joint, (·-·-·-) swing hip joint. (f) Joint's torques: (—) supp. ankle joint, (- - -) supp. shank joint.

k_{Ch1} the number of steps that the robot changes during the walking process from slope to the ground
k_{Ch2} the number of steps that the robot changes during the walking process from the ground to stair

The ranges of the fixed ZMP are selected with respect to the descending and ascending surfaces respectively as follows:

$$-0.05\ \text{m} \leqslant X_{zmp} \leqslant 0.26\ \text{m}$$

$$-0.1\ \text{m} \leqslant X_{zmp} \leqslant 0.26\ \text{m}.$$

In the designed software, these methods are used to simulate the robot including AVI (audio and video interface) files for each identified condition by the users. Differentiating and also using the mathematical methods in the program, the angular velocities and accelerations of the robot's links are calculated to use in the ZMP, Lagrangian and Newtonian equations Table 1.

4. Simulation results

For the described process, the software has been designed based on the cited mathematical methods for simulation of a seven link biped robot. Because of the very high precision of third-order spline method, this method has been applied to calculate the trajectory paths of the robot. The result is 14,000 lines of program in the MATLAB/SIMULINK environment for simulation and stability analysis of the biped robot. By choosing the type of the ZMP in the Fixed and Moving modes, stability analysis of the robot can be judged easily. For the fixed type of ZMP, the torso's modified motion has been regarded to be identical with respect to various phases of the robot's motion. The results have been displayed in Figs. 6–11. Figs. 6–8 present the combined trajectory paths for nominal and non-nominal (with changed hip heights from nominal values) walking of the robot over ascending surfaces. Figs. 9–11 present the same types of walking process over descending surfaces. Both ZMPs have been displayed and their effects on the joint's actuator torques are presented. The impact of swing leg and the ground has been included in the designed software [13,16–18].

5. Conclusion

In this article, combined trajectory paths of a seven link biped robot over various surfaces have been simulated. The saggital movement of the robot has been investigated while 3D simulations of the robot are presented. From the presented simulations, one can observe important parameters of the robot with respect to stability treatment and optimum driver torques. The most important factor is the hip height measured from the fixed coordinate system. As can be seen from Fig. 7f, the support knee needs more actuator torque than the value of the non-nominal gait (with lower hip height measured from the fixed coordinate system). This point can be seen in Figs. 8f and 10f. This is due to the robot's need to bend its knee joint more at a lower hip position.

The role of the hip height is considerable over the torso's modified motion for obtaining the desired fixed ZMP position. With respect to Figs. 10c and 11c, the robot with the lower hip height needs more modified motion of its torso to satisfy the defined ranges of ZMP by the users. The magnitude of the torso's modified motion has drastic effects upon the control process of the robot. Assuming control process of an inverse pendulum included a stagnant origin will present relatively sophisticated control process for substantial deflection angle of pendulum. Note that the torso motion in a biped (as an inverted pendulum) includes both the rotational and translational movements which will complicate the process of control. Consequently, the lower torso's modified motion is desirable which can be derived from the higher hip height. Therefore, the hip height plays an important role in both the stability and optimum actuator torques of the joints. Meanwhile, the higher hip height will avoid the link's velocity discontinuities.

Appendix A. Phases

–First [14] and fifth phases:

$$\theta_a(t) = \begin{cases} -q_{gs} & t = kT_c \\ -q_b & t = kT_c + T_d \\ q_f & t = (k+1)T_c \\ q_{gf} & t = (k+1)T_c + T_d. \end{cases} \tag{1}$$

–Second phase:

$$\theta_a(t) = \begin{cases} -q_{gs} & t = kT_c \\ -q_b & t = kT_c + T_d \\ q_f + \lambda & t = (k+1)T_c \\ q_{gf} + \lambda & t = (k+1)T_c + T_d. \end{cases} \tag{2}$$

–Third phase:

$$\theta_a(t) = \begin{cases} -q_{gs} + \lambda & t = kT_c \\ -q_b + \lambda & t = kT_c + T_d \\ q_f + \lambda & t = (k+1)T_c \\ q_{gf} + \lambda & t = (k+1)T_c + T_d. \end{cases} \tag{3}$$

–Fourth phase:

$$\theta_a(t) = \begin{cases} -q_{gs} + \lambda & t = kT_c \\ -q_b + \lambda & t = kT_c + T_d \\ q_f & t = (k+1)T_c \\ q_{gf} & t = (k+1)T_c + T_d. \end{cases} \tag{4}$$

Appendix B. Horizontal displacement

–First phase [14]:

$$x_{a\ \text{level ground}}(t) = \begin{cases} kD_s & t = kT_c \\ kD_s + l_{an}\ \sin\ q_b + \cdots & t = kT_c + T_d \\ l_{af}(1 - \cos\ q_b) & \\ kD_s + L_{ao} & t = kT_c + T_m \\ (k+2)D_s - l_{an}\ \sin\ q_f - \cdots & t = (k+1)T_c \\ l_{ab}(1 - \cos q_f) & \\ (k+2)D_s & t = (k+1)T_c + T_d. \end{cases} \tag{6}$$

–Second phase:

$$x_{a\ \text{transient11}}(t) = \begin{cases} k_{Ch}D_s & t = kT_c \\ k_{Ch}D_s + l_{an}\sin q_b + \cdots & t = kT_c + T_d \\ l_{af}(1 - \cos q_b) & \\ k_{Ch}D_s + L_{ao} & t = kT_c + T_m \\ (k_{Ch}+1)D_s + (D_s - l_{ab})\cos\lambda - \cdots & t = (k+1)T_c \\ l_{an}\sin(q_f + \lambda) + l_{ab}\cos(q_f + \lambda) & \\ (k_{Ch}+1)D_s + D_s\cos\lambda - \cdots & \\ l_{an}\sin q_f & t = (k+1)T_c + T_d. \end{cases} \tag{7}$$

–Third phase:

$$x_{\mathrm{a,transient11}}(t)=\begin{cases}(k_{\mathrm{Ch}}+1)D_{\mathrm{s}} & t=kT_{\mathrm{c}}\\ (k_{\mathrm{Ch}}+1)D_{\mathrm{s}}+l_{\mathrm{an}}\sin q_{\mathrm{b}}+\cdots & t=kT_{\mathrm{c}}+T_{\mathrm{d}}\\ l_{\mathrm{af}}(1-\cos\ q_{\mathrm{b}}) & \\ (k_{\mathrm{Ch}}+1)D_{\mathrm{s}}+L_{\mathrm{ao}}\cos\ \lambda & t=kT_{\mathrm{c}}+T_{\mathrm{m}}\\ (k_{\mathrm{Ch}}+1)D_{\mathrm{s}}+(2D_{\mathrm{s}}-l_{\mathrm{ab}})\cos\ \lambda-\cdots & t=(k+1)T_{\mathrm{c}}\\ l_{\mathrm{an}}\sin(q_{\mathrm{f}}+\lambda)+l_{\mathrm{ab}}\cos(q_{\mathrm{f}}+\lambda) & \\ (k_{\mathrm{Ch}}+1)D_{\mathrm{s}}+2D_{\mathrm{s}}\cos\lambda-\cdots & \\ l_{\mathrm{an}}\ \sin\ q_{\mathrm{f}} & t=(k+1)T_{\mathrm{c}}+T_{\mathrm{d}}.\end{cases}\tag{8}$$

–Fourth phase:

$$x_{\mathrm{a,Dec}}(t)=\begin{cases}(k_{\mathrm{Ch}}+1)D_{\mathrm{s}}+\mathrm{Dec}_{\mathrm{st}}D_{\mathrm{s}}\cos\lambda-\cdots & t=kT_{\mathrm{c}}\\ l_{\mathrm{an}}\sin\lambda & \\ (k_{\mathrm{Ch}}+1)D_{s_{\mathrm{s}}}+\cdots & t=kT_{\mathrm{c}}+T_{\mathrm{d}}\\ (\mathrm{Dec}_{\mathrm{st}}D_{\mathrm{s}}+l_{\mathrm{af}})\cos\ \lambda-\cdots & \\ l_{\mathrm{af}}\cos(q_{\mathrm{b}}-\lambda)+l_{\mathrm{an}}\cos(q_{\mathrm{b}}-\lambda) & \\ (k_{\mathrm{Ch}}+1)D_{\mathrm{s}}+(\mathrm{Dec}_{\mathrm{st}}D_{\mathrm{s}}+L_{\mathrm{ao}})\cos\lambda & t=kT_{\mathrm{c}}+T_{\mathrm{m}}\\ (k_{\mathrm{Ch}}+1)D_{\mathrm{s}}+\cdots & t=(k+1)T_{\mathrm{c}}\\ ((\mathrm{Dec}_{\mathrm{st}}+2)D_{\mathrm{s}}-l_{\mathrm{ab}})\cos\lambda-\cdots & \\ l_{\mathrm{an}}\sin(q_{\mathrm{f}}+\lambda)+l_{\mathrm{ab}}\ \cos(q_{\mathrm{f}}+\lambda) & \\ (k_{\mathrm{Ch}}+1)D_{\mathrm{s}}+\cdots & t=(k+1)T_{\mathrm{c}}+T_{\mathrm{d}}\\ (\mathrm{Dec}_{\mathrm{st}}+2)D_{\mathrm{s}}\cos\lambda-\cdots & \\ l_{\mathrm{an}}\sin q_{\mathrm{f}}. & \end{cases}\tag{9}$$

–Fifth phase:

$$x_{\mathrm{a,tran.2}}(t)=\begin{cases}(k_{\mathrm{Ch}}+1)D_{\mathrm{s}}+\cdots & t=kT_{\mathrm{c}}\\ (\mathrm{Dec}_{\mathrm{st}}+1)D_{\mathrm{s}}\cos\lambda-l_{\mathrm{an}}\sin\lambda & \\ (k_{\mathrm{Ch}}+1)D_{s_{\mathrm{s}}}+\cdots & t=kT_{\mathrm{c}}+T_{\mathrm{d}}\\ ((\mathrm{Dec}_{\mathrm{st}}+1)D_{\mathrm{s}}+l_{\mathrm{af}})\cos\lambda-\cdots & \\ l_{\mathrm{af}}\cos(q_{\mathrm{b}}-\lambda)+l_{\mathrm{an}}\cos(q_{\mathrm{b}}-\lambda) & \\ (k_{\mathrm{Ch}}+1)D_{\mathrm{s}}+\cdots & t=kT_{\mathrm{c}}+T_{\mathrm{m}}\\ ((\mathrm{Dec}_{\mathrm{st}}+1)D_{\mathrm{s}}+L_{\mathrm{ao}})\cos\lambda & \\ (k_{\mathrm{Ch}}+1)D_{\mathrm{s}}+\cdots & t=(k+1)T_{\mathrm{c}}\\ ((k_{\mathrm{Ch2}}-k_{\mathrm{Ch1}})D_{\mathrm{s}})\cos\lambda+D_{\mathrm{s}}+\cdots & \\ l_{\mathrm{ab}}(\cos q_{\mathrm{f}}-1)-l_{\mathrm{an}}\sin q_{\mathrm{f}} & \\ (k_{\mathrm{Ch}}+1)D_{\mathrm{s}}+\cdots & t=(k+1)T_{\mathrm{c}}+T_{\mathrm{d}}\\ (k_{\mathrm{Ch2}}-k_{\mathrm{Ch1}})D_{\mathrm{s}}\cos\lambda+D_{\mathrm{s}}. & \end{cases}\tag{10}$$

–Sixth phase:

$$x_{\mathrm{a,tran.2}}(t)=\begin{cases}(k_{\mathrm{Ch}}+1)D_{\mathrm{s}}+\cdots & t=kT_{\mathrm{c}}\\ (\mathrm{Dec}_{\mathrm{st}}+2)D_{\mathrm{s}}\cos\lambda-l_{\mathrm{an}}\sin\lambda & \\ (k_{\mathrm{Ch}}+1)D_{s_{\mathrm{s}}}+\cdots & t=kT_{\mathrm{c}}+T_{\mathrm{d}}\\ ((\mathrm{Dec}_{\mathrm{st}}+2)D_{\mathrm{s}}+l_{\mathrm{af}})\cos\lambda-\cdots & \\ l_{\mathrm{af}}\cos(q_{\mathrm{b}}-\lambda)+l_{\mathrm{an}}\cos(q_{\mathrm{b}}-\lambda) & \\ (k_{\mathrm{Ch}}+1)D_{\mathrm{s}}+\cdots & t=kT_{\mathrm{c}}+T_{\mathrm{m}}\\ ((k_{\mathrm{Ch2}}-k_{\mathrm{Ch1}})D_{\mathrm{s}})\cos\lambda+L_{\mathrm{ao}} & \\ (k_{\mathrm{Ch}}+1)D_{\mathrm{s}}+\cdots & t=(k+1)T_{\mathrm{c}}\\ ((k_{\mathrm{Ch2}}-k_{\mathrm{Ch1}})D_{\mathrm{s}})\cos\lambda+2D_{\mathrm{s}}+\cdots & \\ l_{\mathrm{ab}}(\cos q_{\mathrm{f}}-1)-l_{\mathrm{an}}\sin q_{\mathrm{f}} & \\ (k_{\mathrm{Ch}}+1)D_{\mathrm{s}}+\cdots & t=(k+1)T_{\mathrm{c}}+T_{\mathrm{d}}\\ (k_{\mathrm{Ch2}}-k_{\mathrm{Ch1}})D_{\mathrm{s}}\cos\lambda+2D_{\mathrm{s}}. & \end{cases}\tag{11}$$

–Seventh phase:

$$x_{\mathrm{a,level\ ground}}(t)=\begin{cases}(k_{\mathrm{Ch}}+1)D_{\mathrm{s}}+\cdots & t=kT_{\mathrm{c}}\\ ((k_{\mathrm{Ch2}}-k_{\mathrm{Ch1}})D_{\mathrm{s}})\cos\lambda+Lev_{\mathrm{st}}D_{\mathrm{s}} & \\ (k_{\mathrm{Ch}}+1)D_{s_{\mathrm{s}}}+\cdots & t=kT_{\mathrm{c}}+T_{\mathrm{d}}\\ ((k_{\mathrm{Ch2}}-k_{\mathrm{Ch1}})D_{\mathrm{s}})\cos\lambda+Lev_{\mathrm{st}}D_{\mathrm{s}}-\cdots & \\ l_{\mathrm{af}}(1-\cos q_{\mathrm{b}})+l_{\mathrm{an}}\cos q_{\mathrm{b}} & \\ (k_{\mathrm{Ch}}+1)D_{\mathrm{s}}+\cdots & t=kT_{\mathrm{c}}+T_{\mathrm{m}}\\ ((k_{\mathrm{Ch2}}-k_{\mathrm{Ch1}})D_{\mathrm{s}})\cos\lambda+Lev_{\mathrm{st}}D_{\mathrm{s}}+L_{\mathrm{ao}} & \\ (k_{\mathrm{Ch}}+1)D_{\mathrm{s}}+\cdots & t=(k+1)T_{\mathrm{c}}\\ ((k_{\mathrm{Ch2}}-k_{\mathrm{Ch1}})D_{\mathrm{s}})\cos\lambda+(Lev_{\mathrm{st}}+2)D_{\mathrm{s}}+\cdots & \\ l_{\mathrm{ab}}(\cos q_{\mathrm{f}}-1)-l_{\mathrm{an}}\sin q_{\mathrm{f}} & \\ (k_{\mathrm{Ch}}+1)D_{\mathrm{s}}+\cdots & t=(k+1)T_{\mathrm{c}}+T_{\mathrm{d}}\\ (k_{\mathrm{Ch2}}-k_{\mathrm{Ch1}})D_{\mathrm{s}}\cos\lambda+(Lev_{\mathrm{st}}+2)D_{\mathrm{s}}. & \end{cases}\tag{12}$$

Appendix C. Vertical displacement

–First phase [14]:

$$z_{\mathrm{a,\ levelground}}(t)=\begin{cases}h_{\mathrm{gs}}+l_{\mathrm{an}} & t=kT_{\mathrm{c}}\\ h_{\mathrm{gs}}+l_{\mathrm{af}}\sin q_{\mathrm{b}}+l_{\mathrm{an}}\cos q_{\mathrm{b}} & t=kT_{\mathrm{c}}+T_{\mathrm{d}}\\ H_{\mathrm{ao}} & t=kT_{\mathrm{c}}+T_{\mathrm{m}}\\ h_{\mathrm{ge}}+l_{\mathrm{ab}}\sin q_{\mathrm{f}}+l_{\mathrm{an}}\cos q_{\mathrm{f}} & t=(k+1)T_{\mathrm{c}}\\ h_{\mathrm{ge}}+l_{\mathrm{an}} & t=(k+1)T_{\mathrm{c}}+T_{\mathrm{d}}.\end{cases}\tag{13}$$

–Second phase:

$$z_{\mathrm{a,transient1}}(t)=\begin{cases}h_{\mathrm{gs}}+l_{\mathrm{an}} & t=kT_{\mathrm{c}}\\ h_{\mathrm{gs}}+l_{\mathrm{af}}\sin q_{\mathrm{b}}+l_{\mathrm{an}}\cos q_{\mathrm{b}} & t=kT_{\mathrm{c}}+T_{\mathrm{d}}\\ H_{\mathrm{ao}} & t=kT_{\mathrm{c}}+T_{\mathrm{m}}\\ (D_{\mathrm{s}}-l_{\mathrm{ab}})\sin\lambda+\cdots & t=(k+1)T_{\mathrm{c}}\\ l_{\mathrm{ab}}\sin(q_{\mathrm{f}}+\lambda)+l_{\mathrm{an}}\cos(q_{\mathrm{f}}+\lambda) & \\ D_{\mathrm{s}}\sin\lambda+l_{\mathrm{an}}\cos\lambda & t=(k+1)T_{\mathrm{c}}+T_{\mathrm{d}}.\end{cases}\tag{14}$$

–Third phase:

$$z_{\mathrm{a,transient1}}(t)=\begin{cases} h_{\mathrm{gs}}+l_{\mathrm{an}} & t=kT_{\mathrm{c}} \\ D_{\mathrm{s}}\sin\lambda+l_{\mathrm{an}}\cos\lambda & t=kT_{\mathrm{c}}+T_{\mathrm{d}} \\ L_{\mathrm{ao}}\sin\lambda+H_{\mathrm{ao}}\cos\lambda & t=kT_{\mathrm{c}}+T_{\mathrm{m}} \\ (2D_{\mathrm{s}}-l_{\mathrm{ab}})\sin\lambda+\cdots & t=(k+1)T_{\mathrm{c}} \\ l_{\mathrm{ab}}\sin(q_{\mathrm{f}}+\lambda)+l_{\mathrm{an}}\cos(q_{\mathrm{f}}+\lambda) & \\ 2D_{\mathrm{s}}\sin\lambda+l_{\mathrm{an}}\cos\lambda & t=(k+1)T_{\mathrm{c}}+T_{\mathrm{d}}. \end{cases} \tag{15}$$

–Fourth phase:

$$z_{\mathrm{a,Dec}}(t)=\begin{cases} \mathrm{Dec}_{\mathrm{st}}D_{\mathrm{s}}\sin\lambda+l_{\mathrm{an}}\cos\lambda & t=kT_{\mathrm{c}} \\ (\mathrm{Dec}_{\mathrm{st}}D_{\mathrm{s}}+l_{\mathrm{af}})\sin\lambda+\cdots & t=kT_{\mathrm{c}}+T_{\mathrm{d}} \\ l_{\mathrm{af}}\sin(q_{\mathrm{b}}-\lambda)+l_{\mathrm{an}}\cos(q_{\mathrm{b}}-\lambda) & \\ (\mathrm{Dec}_{\mathrm{st}}D_{\mathrm{s}}+L_{\mathrm{ao}})\sin\lambda+\cdots & t=kT_{\mathrm{c}}+T_{\mathrm{m}} \\ H_{\mathrm{ao}}\cos\lambda & \\ ((\mathrm{Dec}_{\mathrm{st}}+2)D_{\mathrm{s}}-l_{\mathrm{ab}})\sin\lambda+\cdots & t=(k+1)T_{\mathrm{c}} \\ l_{\mathrm{ab}}\sin(q_{\mathrm{f}}+\lambda)+l_{\mathrm{an}}\cos(q_{\mathrm{f}}+\lambda) & \\ (\mathrm{Dec}_{\mathrm{st}}+2)D_{\mathrm{s}}\sin\lambda+\cdots & t=(k+1)T_{\mathrm{c}}+T_{\mathrm{d}} \\ l_{\mathrm{an}}\cos\lambda. & \end{cases} \tag{16}$$

–Fifth phase:

$$z_{\mathrm{a,tran.2}}(t)=\begin{cases} (\mathrm{Dec}_{\mathrm{st}}+1)D_{\mathrm{s}}\sin\lambda+l_{\mathrm{an}}\cos\lambda & t=kT_{\mathrm{c}} \\ ((\mathrm{Dec}_{\mathrm{st}}+1)D_{\mathrm{s}}+l_{\mathrm{af}})\sin\lambda+\cdots & t=kT_{\mathrm{c}}+T_{\mathrm{d}} \\ l_{\mathrm{af}}\sin(q_{\mathrm{b}}-\lambda)+l_{\mathrm{an}}\cos(q_{\mathrm{b}}-\lambda) & \\ ((k_{\mathrm{Ch2}}-k_{\mathrm{Ch1}})D_{\mathrm{s}})\sin\lambda+\cdots & t=kT_{\mathrm{c}}+T_{\mathrm{m}} \\ H_{\mathrm{ao}} & \\ ((k_{\mathrm{Ch}}-k_{\mathrm{Ch1}})D_{\mathrm{s}})\sin\lambda+\cdots & t=(k+1)T_{\mathrm{c}} \\ l_{\mathrm{ab}}\sin(q_{\mathrm{f}})+l_{\mathrm{an}}\cos(q_{\mathrm{f}}) & \\ ((k_{\mathrm{Ch2}}-k_{\mathrm{Ch1}})D_{\mathrm{s}})\sin\lambda+\cdots & t=(k+1)T_{\mathrm{c}}+T_{\mathrm{d}} \\ l_{\mathrm{an}}. & \end{cases} \tag{17}$$

–Sixth phase:

$$z_{\mathrm{a,tran.2}}(t)=\begin{cases} (\mathrm{Dec}_{\mathrm{st}}+2)D_{\mathrm{s}}\sin\lambda+l_{\mathrm{an}}\cos\lambda & t=kT_{\mathrm{c}} \\ ((\mathrm{Dec}_{\mathrm{st}}+2)D_{\mathrm{s}}+l_{\mathrm{af}})\sin\lambda+\cdots & t=kT_{\mathrm{c}}+T_{\mathrm{d}} \\ l_{\mathrm{af}}\sin(q_{\mathrm{b}}-\lambda)+l_{\mathrm{an}}\cos(q_{\mathrm{b}}-\lambda) & \\ ((k_{\mathrm{Ch2}}-k_{\mathrm{Ch1}})D_{\mathrm{s}})\sin\lambda+\cdots & t=kT_{\mathrm{c}}+T_{\mathrm{m}} \\ H_{\mathrm{ao}} & \\ ((k_{\mathrm{Ch}}-k_{\mathrm{Ch1}})D_{\mathrm{s}})\sin\lambda+\cdots & t=(k+1)T_{\mathrm{c}} \\ l_{\mathrm{ab}}\sin(q_{\mathrm{f}})+l_{\mathrm{an}}\cos(q_{\mathrm{f}}) & \\ ((k_{\mathrm{Ch2}}-k_{\mathrm{Ch1}})D_{\mathrm{s}})\sin\lambda+\cdots & t=(k+1)T_{\mathrm{c}}+T_{\mathrm{d}} \\ l_{\mathrm{an}}. & \end{cases} \tag{18}$$

–Seventh phase:

$$z_{\text{a,level 2ground}}(t)=\begin{cases}((k_{\text{Ch2}}-k_{\text{Ch1}})D_{\text{s}})\sin\lambda+l_{\text{an}} & t=kT_{\text{c}}\\ ((k_{\text{Ch2}}-k_{\text{Ch1}})D_{\text{s}})\sin\lambda+\cdots & t=kT_{\text{c}}+T_{\text{d}}\\ l_{\text{af}}\sin(q_{\text{b}})+l_{\text{an}}\cos(q_{\text{b}})\\ ((k_{\text{Ch2}}-k_{\text{Ch1}})D_{\text{s}})\sin\lambda+\cdots & t=kT_{\text{c}}+T_{\text{m}}\\ H_{\text{ao}} & \\ ((k_{\text{Ch}}-k_{\text{Ch1}})D_{\text{s}})\sin\lambda+\cdots & t=(k+1)T_{\text{c}}\\ l_{\text{ab}}\sin(q_{\text{f}})+l_{\text{an}}\cos(q_{\text{f}})\\ ((k_{\text{Ch2}}-k_{\text{Ch1}})D_{\text{s}})\sin\lambda+\cdots & t=(k+1)T_{\text{c}}+T_{\text{d}}\\ l_{\text{an}}.\end{cases}\tag{19}$$

–Eighth phase:

$$z_{\text{a,stair,descending}}(t)=\begin{cases}((k_{\text{Ch2}}-k_{\text{Ch1}})D_{\text{s}})\sin\lambda+l_{\text{an}} & t=kT_{\text{c}}\\ ((k_{\text{Ch2}}-k_{\text{Ch1}})D_{\text{s}})\sin\lambda+\cdots & t=kT_{\text{c}}+T_{\text{d}}\\ l_{\text{af}}\sin(q_{\text{b}})+l_{\text{an}}\cos(q_{\text{b}})\\ ((k_{\text{Ch2}}-k_{\text{Ch1}})D_{\text{s}})\sin\lambda+\cdots & t=kT_{\text{c}}+T_{\text{m}}\\ H_{\text{ao}} & \\ ((k_{\text{Ch}}-k_{\text{Ch1}})D_{\text{s}})\sin\lambda+\cdots & t=(k+1)T_{\text{c}}\\ l_{\text{ab}}\sin(q_{\text{f}})+l_{\text{an}}\cos(q_{\text{f}})+h_{\text{s}}\\ ((k_{\text{Ch2}}-k_{\text{Ch1}})D_{\text{s}})\sin\lambda+\cdots & t=(k+1)T_{\text{c}}+T_{\text{d}}\\ l_{\text{an}}+h_{\text{s}}.\end{cases}\tag{20}$$

–Ninth phase:

$$z_{\text{a,stair,descending}}(t)=\begin{cases}((k_{\text{Ch2}}-k_{\text{Ch1}})D_{\text{s}})\sin\lambda+l_{\text{an}} & t=kT_{\text{c}}\\ ((k_{\text{Ch2}}-k_{\text{Ch1}})D_{\text{s}})\sin\lambda+\cdots & t=kT_{\text{c}}+T_{\text{d}}\\ l_{\text{af}}\sin(q_{\text{b}})+l_{\text{an}}\cos(q_{\text{b}})\\ ((k_{\text{Ch2}}-k_{\text{Ch1}})D_{\text{s}})\sin\lambda+\cdots & t=kT_{\text{c}}+T_{\text{m}}\\ H_{\text{ao}} & \\ ((k_{\text{Ch}}-k_{\text{Ch1}})D_{\text{s}})\sin\lambda+\cdots & t=(k+1)T_{\text{c}}\\ l_{\text{ab}}\sin(q_{\text{f}})+l_{\text{an}}\cos(q_{\text{f}})+2h_{\text{s}}\\ ((k_{\text{Ch2}}-k_{\text{Ch1}})D_{\text{s}})\sin\lambda+\cdots & t=(k+1)T_{\text{c}}+T_{\text{d}}\\ l_{\text{an}}+2h_{\text{s}}.\end{cases}\tag{21}$$

–Tenth phase:

$$z_{\text{a,stair,descending}}(t)=\begin{cases}((k_{\text{Ch2}}-k_{\text{Ch1}})D_{\text{s}})\sin\lambda+\cdots & t=kT_{\text{c}}\\ l_{\text{an}}-\text{St}_{con}h_{\text{s}}\\ ((k_{\text{Ch2}}-k_{\text{Ch1}})D_{\text{s}})\sin\lambda+\cdots & t=kT_{\text{c}}+T_{\text{d}}\\ l_{\text{af}}\sin(q_{\text{b}})+l_{\text{an}}\cos(q_{\text{b}})+\text{St}_{con}h_{\text{s}}\\ ((k_{\text{Ch2}}-k_{\text{Ch1}})D_{\text{s}})\sin\lambda+\cdots & t=kT_{\text{c}}+T_{\text{m}}\\ -(\text{St}_{con}+1)h_{\text{s}}+H_{\text{s}}\\ ((k_{\text{Ch2}}-k_{\text{Ch1}})D_{\text{s}})\sin\lambda+\cdots & t=(k+1)T_{\text{c}}\\ l_{\text{ab}}\sin(q_{\text{f}})+l_{\text{an}}\cos(q_{\text{f}})+(\text{St}_{con}+2)h_{\text{s}}\\ ((k_{\text{Ch2}}-k_{\text{Ch1}})D_{\text{s}})\sin\lambda+\cdots & t=(k+1)T_{\text{c}}+T_{\text{d}}\\ l_{\text{an}}-(\text{St}_{con}+2)h_{\text{s}}.\end{cases}\tag{22}$$

References

[1] P.N. Mousavi, A. Bagheri, Mathematical simulation of a seven link biped robot on various surfaces and ZMP considerations, Applied Mathematical Modelling, vol. 31/1, Elsevier, 2007, pp. 18–37.
[2] M.Y. Zarrugh, C.W. Radcliffe, Computer generation of human gait kinematics, J. Biomech. 12 (1979) 99–111.
[3] T. McGeer, Passive walking with knees, in: Proc. IEEE Int. Conf. Robotics and Automation, 1990, pp. 1640–1645.
[4] F.M. Silva, J.A.T. Machado, Energy analysis during biped walking, in: Proc. IEEE Int. Conf. Robotics and Automation, 1999, pp. 59–64.
[5] Y.F. Zheng, J. Shen, Gait synthesis for the SD-2 biped robot to climb sloping surface, IEEE Trans. Robot. Automat. 6 (1990) 86–96.
[6] C. Chevallereau, A. Formal'sky, B. Perrin, Low energy cost reference trajectories for a biped robot, in: Proc. IEEE Int. Conf. Robotics and Automation, 1998, pp. 1398–1404.
[7] A. Takanishi, M. Ishida, Y. Yamazaki, I. Kato, The realization of dynamic walking robot WL-10RD, in: Proc. Int. Conf. Advanced Robotics, 1985, pp. 459–466.
[8] C.L. Shih, Y.Z. Li, S. Churng, T.T. Lee, W.A. Cruver, Trajectory synthesis and physical admissibility for a biped robot during the single support phase, in: Proc. IEEE Int. Conf. Robotics and Automation, 1990, pp. 1646–1652.
[9] K. Hirai, M. Hirose, Y. Haikawa, T. Takenaka, The development of Honda humanoid robot, in: Proc. IEEE Int. Conf. Robotics and Automation, 1998, pp. 1321–1326.
[10] A. Dasgupta, Y. Nakamura, Making feasible walking motion of humanoid robots from human motion capture data, in: Proc. IEEE Int. Conf. Robotics and Automation, 1999, pp. 1044–1049.
[11] C. Shih, Gait synthesis for a biped robot, Robotica 15 (1997) 599–607.
[12] C.L. Shih, Ascending and descending stairs for a biped robot, IEEE Trans. Syst. Man. Cybern. A 29 (3) (1999) 255–268.
[13] Q. Huang, K. Yokoi, S. Kajita, K. Kaneko, H. Arai, N. Koyachi, K. Tanie, Planning walking patterns for a biped robot, IEEE Trans. Robot. Automat. 17 (3) (2001).
[14] P.N. Mousavi, Adaptive Control of 5 DOF Biped Robot Moving on a Declined Surface, M.S. Thesis, Guilan University, 2006.
[15] J.G. John, Introduction to Robotics: Mechanics and Control, Addison-Wesley, 1989.
[16] H.K. Lum, M. Zribi, Y.C. Soh, Planning and contact of a biped robot, Int. J. Eng. Sci. 37 (1999) 1319–1349.
[17] Eric R. Westervelt, Toward a coherent framework for the control of plannar biped locomotion, A Dissertation Submitted in Partial Fulfillment of the Requirements for the Degree of Doctor of Philosophy, (Electrical Engineering Systems), the University of Michigan, 2003.
[18] H. Hon, T. Kim, T. Park, Tolerance analysis of a Spur gear train, in: Proc. Third DADS Korean User's Conf. 1978, pp. 61–81.